



# Microfluidic Study of Synergic Liquid-Liquid Extraction of Rare Earth Elements

Asmae El Maangar, Johannes Theisen, Christophe Penisson, Thomas Zemb, Jean-Christophe P Gabriel

## ► To cite this version:

Asmae El Maangar, Johannes Theisen, Christophe Penisson, Thomas Zemb, Jean-Christophe P Gabriel. Microfluidic Study of Synergic Liquid-Liquid Extraction of Rare Earth Elements. *Physical Chemistry Chemical Physics*, 2020, 22, pp.5449-5462. 10.1039/C9CP06569E . cea-02476112

**HAL Id: cea-02476112**

**<https://cea.hal.science/cea-02476112>**

Submitted on 12 Feb 2020

**HAL** is a multi-disciplinary open access archive for the deposit and dissemination of scientific research documents, whether they are published or not. The documents may come from teaching and research institutions in France or abroad, or from public or private research centers.

L'archive ouverte pluridisciplinaire **HAL**, est destinée au dépôt et à la diffusion de documents scientifiques de niveau recherche, publiés ou non, émanant des établissements d'enseignement et de recherche français ou étrangers, des laboratoires publics ou privés.



Distributed under a Creative Commons Attribution - NonCommercial 4.0 International License

# PCCP

Physical Chemistry Chemical Physics

Accepted Manuscript

This article can be cited before page numbers have been issued, to do this please use: A. EL MAANGAR, J. Theisen, C. Penisson, T. Zemb and J. P. GABRIEL, *Phys. Chem. Chem. Phys.*, 2020, DOI: 10.1039/C9CP06569E.



This is an Accepted Manuscript, which has been through the Royal Society of Chemistry peer review process and has been accepted for publication.

Accepted Manuscripts are published online shortly after acceptance, before technical editing, formatting and proof reading. Using this free service, authors can make their results available to the community, in citable form, before we publish the edited article. We will replace this Accepted Manuscript with the edited and formatted Advance Article as soon as it is available.

You can find more information about Accepted Manuscripts in the [Information for Authors](#).

Please note that technical editing may introduce minor changes to the text and/or graphics, which may alter content. The journal's standard [Terms & Conditions](#) and the [Ethical guidelines](#) still apply. In no event shall the Royal Society of Chemistry be held responsible for any errors or omissions in this Accepted Manuscript or any consequences arising from the use of any information it contains.

## ARTICLE

## Microfluidic Study of Synergic Liquid-Liquid Extraction of Rare Earth Elements

Asmae El Maangar<sup>a,b</sup>, Johannes Theisen<sup>a,b</sup>, Christophe Penisson<sup>a,b</sup>, Thomas Zemb<sup>b</sup>, and Jean-Christophe P. Gabriel<sup>a,c\*,†</sup>Received 00th January 20xx,  
Accepted 00th January 20xx

DOI: 10.1039/x0xx00000x

A microfluidic technique is associated to X-ray fluorescence in order to investigate the origin of the so-called synergy effect observed in liquid-liquid extraction of rare earth elements (REE) when special combinations of two extractants – one solvating and one ionic – are used. The setup enables kinetic studies by varying the two phases' contact time. Results obtained are compared to those obtained using standard batch extraction method with equal contact time. We then determine variation of free energies of transfer for five rare earth elements present in solution together with a non-target ion ( $\text{Fe}^{3+}$ ) at different pH. Analysis of the effect of temperature, as well as of surface charge density of the coexisting cations, allow separating electrostatic from complexation effects. We finally show that all non-linear (synergic) effects are quadratic in mole fraction. This demonstrates that in-plane mixing entropy of the bent extractant film, in the first nanometer around rare earth ions, is the determining term in the synergy effect. Surprisingly, even when the third phase is present, free energies of transfer could still be measured in the diluted phase, which is reported for the first time, to our knowledge. We hence show that the extractive power of the dense third phase is stronger than conventional reverse aggregates in equilibrium with excess water.

## Introduction

With increased scarcity and/or strategic importance of many chemical elements of the periodic table,<sup>1–4</sup> there is a large thrust in research efforts for new economically viable processes for the recycling of such elements from the “Urban Mine”, *ca.* our wastes.<sup>5–7</sup> A critical example can be found in the case of rare earth elements (REE) that are key elements in so many applications surrounding us, especially in the electronic and energy sector.<sup>3, 8, 9</sup> Many of such processes are based on liquid-liquid extraction,<sup>10–14</sup> hence making use of very complex formulations, often referred to as complex fluids.<sup>13, 15</sup> Ions transfer between two phases and its driving force have been the subject of many kinetic, thermodynamic, theoretical, and modeling studies which require years of research with yet many remaining unknowns.<sup>11, 16–20, 21–22</sup> In addition to this complexity, even when promising hydrometallurgy processes are described, their use by the recycling industry is hindered by the cost associated with the use of very low pH, as well as the variability

in elemental composition from one waste lot to the other. The industry is therefore not only in need for more efficient approaches that can work at higher pH and show higher performances but also of methods enabling faster speed of process development or adjustment. In order to reduce time and volume, relying on microfluidic devices represent a very promising route.<sup>15, 22–30</sup> Indeed, since the pioneering work of Ismagilov and co-workers,<sup>22</sup> microfluidics has developed as a popular method to save quantities of test materials needed to complete experimental plans in formulating efficient processes. The main difficulties in using microfluidics instead of the old “batch” method are related to the adsorption of electrolytes on all interfaces present as well as to the sensitivity required in element analysis. These effects contribute to uncertainty in final result.<sup>31</sup> The precise control of kinetics effects limited by diffusion in thin channels depends on the design strategy chosen (membrane, membrane-less, bubble, droplet). In a preliminary paper, we have shown that the presence of a membrane does not limit the transfer observed and can be considered as an alternative to the most popular strategy based on droplets.<sup>32</sup>

In this paper we report on the interest of chemical analysis of all four microfluidic channels (aqueous/oil, in & out), which enable accurate measurements of concentrations ratio  $[\text{Ion}]_{\text{out}}/[\text{Ion}]_{\text{in}}$  (both in water and oil). We show that such a microfluidic study, here applied to a very promising synergic system formed by two different extracting molecules,<sup>33</sup> allows for: (i) classical yield measurements, but also, and for the first time to our best knowledge; (ii) the measurement of Gibbs free

<sup>a</sup> Institut de Recherche Interdisciplinaire de Grenoble, IRIG, Univ. Grenoble Alpes, IRIG-MEM, F-38000 Grenoble, France.

<sup>b</sup> Institut de Chimie Séparative de Marcoule, ICSM, Univ Montpellier, CEA, CNRS, ENSCM, Marcoule, France.

<sup>c</sup> Nanoscience and Innovation for Materials, Biomedicine and Energy (NIMBE), CEA/CNRS/Univ. Paris-Saclay, CEA Saclay, F-91191 Gif-sur-Yvette.

\* Corresponding authors: JCP Gabriel (jean-christophe.gabriel@cea.fr)

† Current address: Energy Research Institute @ NTU (ERI@N), Nanyang Technological University, Singapore.

Electronic Supplementary Information (ESI) available: [details of any supplementary information available should be included here]. See DOI: 10.1039/x0xx00000x



energies of transfer reaction and thus not only for Winsor II but also Winsor III data points.<sup>14, 34, 35</sup>

## Experimental

### Chemicals

The solvating extractant *N,N'*-dimethyl-*N,N'*-dioctylhexylethoxymalonamide (DMDOHEMA) was purchased from Panchim SARL (Lisses, France) with a purity higher than 99%, determined by gas chromatography coupled to mass spectrometry (GC-MS). The cation exchanger Bis(2-ethylhexyl)phosphoric acid (HDEHP) was purchased from Sigma Aldrich with a purity higher than 97%. Isane® IP175 was purchased from Total Special fluids. Water was deionized using a Millipore Milli-Q purification system (Merck Millipore, Billerica, MA). All other chemicals were purchased from commercial sources: 70% Nitric acid  $\text{HNO}_3$  (Sigma Aldrich), Lanthanum(III) nitrate hexahydrate  $\text{La}(\text{NO}_3)_3 \cdot 6\text{H}_2\text{O}$  (Sigma Aldrich; purity, > 99,99%),

For all samples, organic phases containing both extracting molecules DMDOHEMA and HDEHP were prepared with a well-defined quantity of the two extractants at different molar fractions of DMDOHEMA varying from 0 to 1 in steps of 0.25 (as reported in Table 1 of Supplementary Materials) diluted in Isane® IP175. Solutions of both extractants were prepared so that their total concentration in extractant molecules, ( $C_{\text{tot}} = C_{\text{DMDOHEMA}} + C_{\text{HDEHP}}$ ) was fixed to  $0.9 \text{ mol.L}^{-1}$ . This latter concentration is chosen to be above critical aggregation concentrations (CAC) for both extractants.<sup>33, 36</sup>

In order to measure all selectivities in a simulated although realistic case, we chose a reference aqueous solution composition that contained five lanthanides and a typical non-target ion,  $\text{Fe}^{3+}$ . Ln(III) and iron(III) aqueous solutions were obtained by dissolving  $\text{La}(\text{NO}_3)_3 \cdot 6\text{H}_2\text{O}$ ,  $\text{Nd}(\text{NO}_3)_3 \cdot 6\text{H}_2\text{O}$ ,  $\text{Eu}(\text{NO}_3)_3 \cdot 6\text{H}_2\text{O}$ ,  $\text{Dy}(\text{NO}_3)_3 \cdot 6\text{H}_2\text{O}$ ,  $\text{Yb}(\text{NO}_3)_3 \cdot 6\text{H}_2\text{O}$  and  $\text{Fe}(\text{NO}_3)_3 \cdot 9\text{H}_2\text{O}$ , in an aqueous solution of nitric acid at different

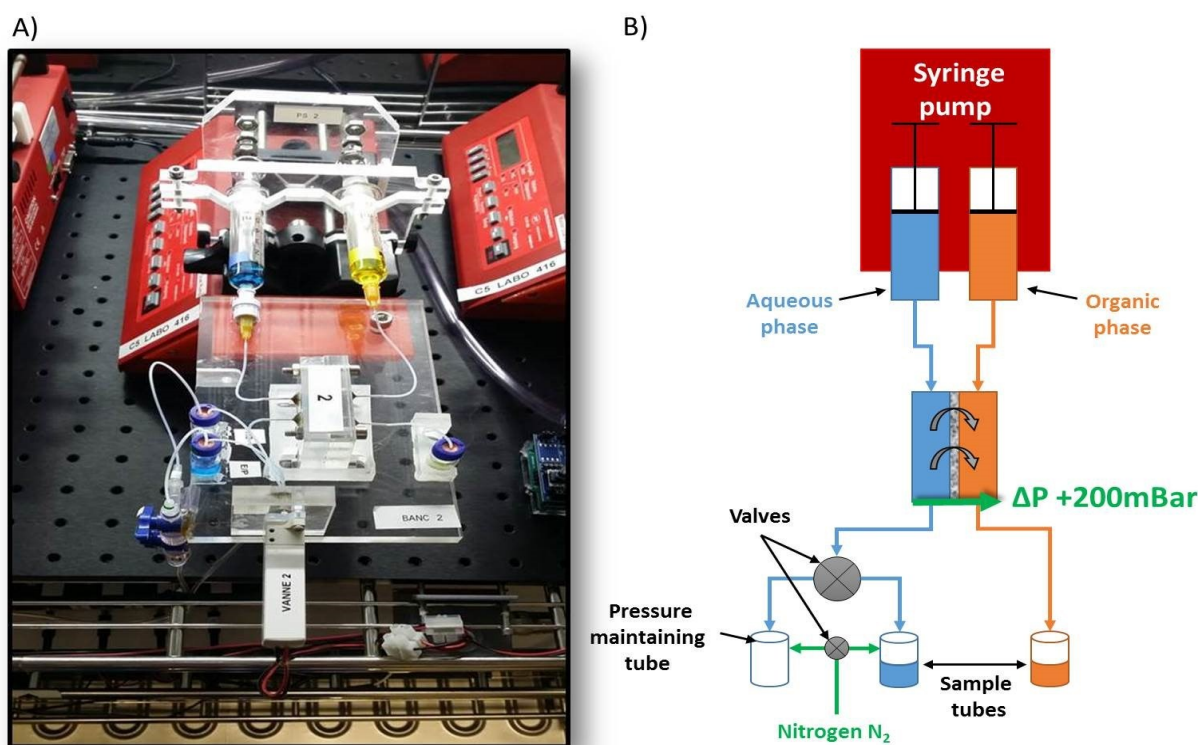


Figure 1: A) photo of the experimental bench with (from top to bottom): syringe pump modified to accommodate two syringes; aqueous (blue liquid) and organic (yellow liquid) syringes; microfluidic extraction chip; aqueous and organic output sample septum vial; valve; artificial food colouring in water is used to enable better visualisation. B) Schematic representation of the microfluidic set-up with injection and extraction cell.

Neodymium(III) nitrate hexahydrate  $\text{Nd}(\text{NO}_3)_3 \cdot 6\text{H}_2\text{O}$  (Sigma Aldrich; purity, > 99,9%), Europium(III) nitrate hexahydrate  $\text{Eu}(\text{NO}_3)_3 \cdot 6\text{H}_2\text{O}$  (Sigma Aldrich; purity, > 99,9%), Dysprosium(III) nitrate hexahydrate  $\text{Dy}(\text{NO}_3)_3 \cdot 6\text{H}_2\text{O}$  (Sigma Aldrich; purity, > 99,9%), Ytterbium(III) nitrate hexahydrate  $\text{Yb}(\text{NO}_3)_3 \cdot 6\text{H}_2\text{O}$  (Sigma Aldrich; purity, > 99,9%) and Iron(III) nitrate nonahydrate  $\text{Fe}(\text{NO}_3)_3 \cdot 9\text{H}_2\text{O}$  (Sigma Aldrich; purity, > 99,999%). All chemical products were used without further purification.

### Solution preparation

concentrations ( $[\text{HNO}_3] = 0.03, 0.3$  and  $3 \text{ M}$ ), so that each of their respective concentrations in the aqueous phase was  $10 \text{ mmol.L}^{-1}$ . The initial concentration of the different salts in the aqueous phase was verified both by X-ray Fluorescence (XRF) and Inductively Coupled Plasma Atomic Emission Spectrophotometry (ICP-OES) analysis.

### Microfluidic system

We used the set-up as illustrated in Figure 1 and previously described in details, as well as validated, elsewhere.<sup>31, 32</sup> Typically, the oil and aqueous channels, are micromachined in





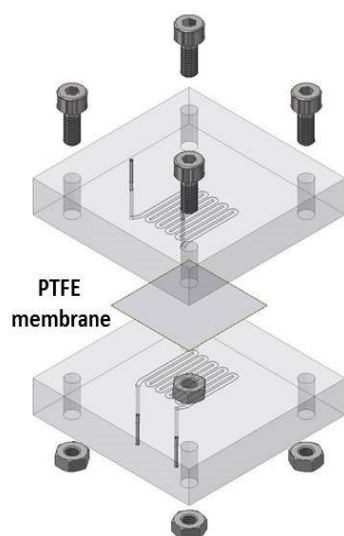


Figure 2: 3D sketch of microfluidic extraction circuit card with: PTFE membrane; four tightening bolts for mechanical stability; PMMA block milled with microfluidic serpentine channels; input/output stainless steel tubes. The volume of each channel within the phases contact area is 35.7  $\mu\text{L}$ . Reprinted from ref. 33, Copyright 2019, with permission from Elsevier.

Poly(methyl methacrylate) (PMMA) blocks, which are chemically compatible with nitric acid and Isane® IP175, that were separated by a hydrophobic and porous PTFE membrane with a thickness of 30  $\mu\text{m}$ , pore size of 20 nm and porosity of 55% (Commercially available from Cobetter filtration, China). It acts as capillary separation between the microfluidic channels. The thickness of this membrane was previously optimised to 30  $\mu\text{m}$  so as: (i) be easy to handle; (ii) not become the limiting factor in the mass transfer kinetics.<sup>32</sup> Connectors between the microfluidic ship and PTFE tubing were made of stainless-steel tubing sealed with epoxy resin (Figure 2).

Our validated microfluidic liquid-liquid extraction procedure can be summarized as follow:<sup>31, 32</sup> the first step of any of our microfluidic extractions consisted in loading the aqueous and oil phases – classically an extractant at predetermined composition and a “diluent” – into gas-tight 5 mL glass syringes equipped with PTFE plunger (Hamilton Bonaduz, syringe 1005TLL). Then, both syringes were placed on a syringe pump (NE1000, New Era Pump Systems, modified to enable simultaneous usage of two syringes) to deliver desired flow rates and injection volumes. Both syringes were connected to the microfluidic device with PTFE tubing of internal diameter 0.65 mm and known overall length. The aqueous sample was introduced first, manually, into the aqueous channel in order to avoid for the organic phase to pass through the membrane. Indeed, this may occur whenever oil phase is introduced first while the aqueous channel is either left empty or if it is under pressurized. Hence, a slight back-pressure of 200 mbar must be applied to the aqueous channel, thus maintaining the oil-water interface within the membrane. This back-pressure was applied by connecting the output sample septum vial to a pressure regulated nitrogen ( $\text{N}_2$ ) reservoir (Figure 1). Then the organic phase was injected into the organic channel. When both microfluidic channels were filled, both syringes were perfused simultaneously and at equal flow rates by computer-controlled automation. For each data

point, the microfluidic device was (i) fully flushed with twice its internal volume, in order to assure reaching a steady state, (ii) further flushed until 600  $\mu\text{L}$  of each phase was retrieved in collecting output vials, for off-line XRF or ICP-OES analysis (see Supplementary Materials for more details about the XRF analysis). Necessary overall time required to obtain each sample varies according to the flow rate used (always equal, by construction, for both phases (Figure 1) which in our case varies from 34  $\mu\text{L}/\text{min}$  to 0.57  $\mu\text{L}/\text{min}$  (see Table 2 of Supplementary Materials). For all experimental studies: (i) both aqueous and organic samples were sampled out for five different contact times between the two phases, ca. after 1, 3, 10, 30, and 60 minutes, respectively. When all flow rates for a given composition have been sampled, the device of Figure 2 was disassembled, cleaned and its membrane replaced to proceed to another composition within the phase diagram. All microfluidic extractions were performed within a large (1  $\text{m}^3$ ) thermostated chamber (Mettler, IPP 750 Plus), regulated at the set experimental temperature  $\pm 0.1^\circ\text{C}$ .

It should be noted that the collection of 600  $\mu\text{L}$  from the microfluidic platform was the main data point acquisition time's limiting factor. Such a large volume was indeed required to perform off-line characterizations. In future implementations, this data point experimental time should be reduced to whichever is the limiting factor: (i) the time required to acquire an on-line XRF spectra, once XRF is integrated to the platform; or (ii) the time to reach a steady state when using very slow flow rates. This will be the case in the next generation of our platform. Other groups have already integrated an online ICP-MS, but with the issue that it only measures the aqueous channel which further often requires a dilution before performing the measurement.<sup>37</sup>

It should be noted that a blank experiment, in which only pure oil –ca. without extracting molecules– was performed and showed that no metals was extracted from the aqueous phase. Such loss of metal can sometime be observed due to their adsorption onto channels' surfaces. This is usually avoided as long as the thickness of the microfluidic channels are more than 0.05 mm. Here, we used channels with rectangular cross-section of 0.4 mm in width and 0.2 mm in depth and with a contact section 171 mm long. Hence we did not need to correct data for adsorbed cations in the porous membrane or elsewhere.

It should be noted that in some cases, organic phase samples obtained at the organic channel output decant in both an extractant-poor and an extractant-rich phases. The latter viscous phase is often referred to as a Winsor III instability, which is at the origin of the so-called “Third phase” incident in hydrometallurgy containing a dense and viscous phase, expelling a lighter and fluid organic phase. This phase separation was not observed by naked eye within the organic channel of the device during extraction process. Due to its increased density, it also leads to a reduced volume for the collected organic sample i.e less than 600  $\mu\text{L}$ . After settling, the two organic phases were separated and recovered by decantation to measure their respective ions concentrations by XRF.



### Batch extractions

Batch extractions were performed in parallel to microfluidic extractions to serve as additional comparison and further validation points. These batch samples were prepared using identical compositions for the initial solutions (fifteen aqueous batch samples to be contacted with fifteen organic batch samples) as previously described in details:<sup>33</sup> typically, we used a 1:1 volume ratio between the aqueous and the organic phases - the volume of each phase being 2.5 mL. Contact time of the two phases within a test tubes was set to 1h, using permanent mechanical shaking, to maintain a good emulsification, at room temperature. In the case of low acidity, extraction kinetic is slower. In order to achieve equilibrium, additional batch extractions were performed for contact times of 120, 180 and 480 min, and associated the recovery factor as calculated.

Then, in all cases, the two phases were separated by centrifugation (8000 rpm for 30 minutes) and recovered separately by decantation. Results were compared to microfluidic extraction having a one hour contact time. All experiments were carried out at room temperature ( $25 \pm 1^\circ\text{C}$ ) or, when other temperatures were studied, in a temperature controlled closed chamber (Mettmert, IPP 750 Plus).

### XRF

The commercial XRF spectrometer used to analyse both aqueous and organic phases after extraction is a SPECTRO XEPOS (AMETEK) model. It is commercially equipped with an energy dispersive X-ray analyser (ED-XRF) that used the energy loss of the X photon in a silicon material to determine the spectrum by a suitable signal processing. Secondary targets reduce background noise compared to the output signal from the tube and improve fluorescence detection. Liquid samples were placed in 6 mm diameter cups, the bases of which consisted of a 4  $\mu\text{m}$  thick prolene film. The XRF spectrometer was used to analyse a series of eleven cups in sequence, using a rotating carousel that positions the sample to be measured above the inverted optical part. A volume of 100  $\mu\text{L}$  for each of the samples was placed in the micro-cups of analysis for a duration of 40 minutes. The X-ray tube generator was set at 40 kV and an intensity of 0.160 mA. The Zirconium secondary target was monitored between 15 and 17 keV to visualize the fluorescence of all lanthanides and iron: between 4 keV and 10 keV.

### ICP-OES

Rare earths extraction was also analysed by ICP-OES: aqueous solution ion concentrations were measured before and after extraction. The commercial tool used for this study is a SPECTRO ARCOS ICP-OES, which is equipped with a circular detector consisting of 32 linearly aligned CCDs, each having a resolution of 3648 pixels covering wavelengths ranging from 130 to 770 nm. The resolution of the detector is 8.5  $\mu\text{m}$  from 130 – 340 nm and 15  $\mu\text{m}$  from 340 – 770 nm with an intensity dynamic range of eight orders of magnitudes. CCDs were read out simultaneously and a complete spectrum was generated under two seconds. The circular polychromator (Paschen-Runge

design, optical components:  $\text{MgF}_2$ , Zerodur structure) has a

DOI: 10.1039/C9CP06569E

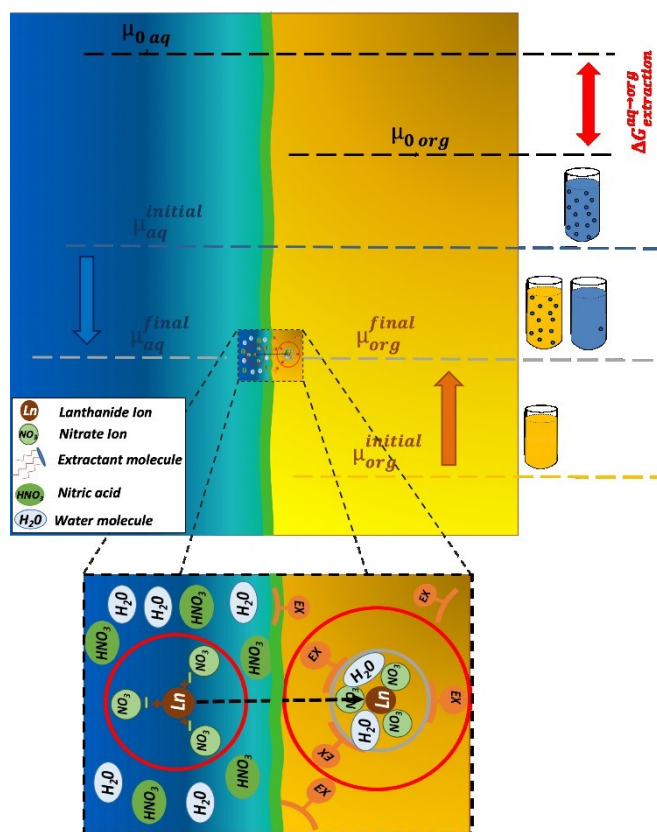


Figure 3: Location of the relative chemical potentials of the electrolyte during liquid-liquid extraction: reference chemical potentials  $\mu^0$  are indicated explicitly. The water rich phase is represented in blue and the oil phase in orange, while the interface, or rather the interphase, is schematized by a thick green undulating line. Extraction of ions into the organic phase is made possible by its incorporation within the core of an aggregate made of extractant molecules. Polar heads of extractant molecules are oriented toward the core of the aggregate.

focal distance of 750 mm. The radio frequency generator works at a frequency of 27.12 MHz and has a power output of 0.7 to 1.7 kW with an efficiency of 70 % and a stability of 0.1 %.

A typical sample analysis was carried out as follows: The sample was diluted to an appropriate concentration ranging between 5 to 15 mg/L using 2%  $\text{HNO}_3$  in water. Before each run a calibration was performed with metal standards made from a calibrated solution (1000 mg/L) which was diluted to obtain standards at 0, 1, 5 and 15 mg/L. Each sample was measured three times for statistical reasons and after each measurement, the system was purged with 2%  $\text{HNO}_3$ .

## Results & Discussion

Currently, there are seventeen identified categories in the strategy for formulating efficient complex fluids for liquid-liquid extraction.<sup>15, 34, 38</sup> The vast majority of these efficient formulations combine a solvating extractant and an ionic exchanger extractant that can modify the overall reaction mechanism and lead to either a synergic or an antagonist effect.<sup>34, 39-42</sup> Synergy -for which no predictive theory exists yet - is strongly affected by various parameters such as aqueous



phase acidity, amount of extractants as well as temperature.<sup>40</sup> Most of these effective processes rely on combining two extractants and an optimized “diluent” with so-called modifiers.<sup>10, 11, 43-46</sup> To optimize a process, both “yield”, expressed in mass extracted by unit of time, and “selectivity” in differentiating “target” from “non-target” elements are considered.<sup>47</sup> In the absence of general predictive theory for the selectivity of multi-component complex fluids,<sup>33, 40, 48</sup> optimization requires very lengthy experimental plans.

Anyhow, selectivity can be understood by comparing the “double differences” of free energies of transfer between the water and the oil phases ( $\Delta\Delta G_R^0$ ) for the two elements considered.<sup>16</sup> The methodology is illustrated in Figure 3, it gives an overview on how an extraction process can be coupled with thermodynamic driving forces. On the left side, the Gibbs free energy of transfer between the water and oil phase is calculated using the ienais approach: from the difference between the reference chemical potentials of each phase (Equation 2) -since the reference chemical potential reflects the intrinsic affinity of the solute towards the aqueous or oil phase -. In Figure 3, the reference chemical potential of a solute in the initial aqueous phase  $\mu_{Aq}^{initial}$  (blue bar) is higher than the reference chemical potential in the final organic phase after contact  $\mu_{Org}^{final}$  (grey bar). Thus, it is transferred into the organic phase, as it is thermodynamically favourable (see reference <sup>16</sup> for further details on the ienais approach). At the input of the microfluidic device, ions have an initial state which is represented by an initial chemical potential in each phase i.e.  $\mu_{Aq}^{initial}$  and  $\mu_{Org}^{initial}$ , during the transfer, the ion will reach thermodynamic equilibrium and will have the same chemical potential in both phases at the output of the liquid-liquid extraction microfluidic zone (Equation 1).

The chemical potential can then be split into the reference chemical potential in the designated phase and a second term related to the activity. Such rearrangement of Equation 1 leads to an expression of the free energy of transfer,  $\Delta G_R^0$  (Equation 2), in which, assuming ideal behaviour (i.e. no interactions of the solute molecules between each other), the activity can be reduced to the solute's concentration. Thus, the free energy of transfer can be expressed using only the ratio of the considered ion's concentration in each individual phase (Equation 3 to Equation 5).

$$\mu_{Aq}^{final} = \mu_{Org}^{final} \quad \text{Equation 1}$$

This explains the final aim of this microfluidic investigation: to explore the phase diagram of a synergic extraction system in regards to its ions free energies of transfer from the water to the oil phase, and thus as fast as the kinetics of the extraction allows (typically from few minutes to few hours in worse cases). Also, since our microfluidic chip allows to precisely control solution's contact times, it therefore also enables studying transient states and establishing extraction's time dependence. Studying such transient behaviours, at constant total molarity of extractant, allows identifying asymptotic values, therefore

characterizing the thermodynamic equilibrium and thus for various acid concentration, temperature and molar fractions. It therefore allows determining the Gibbs free energy of transfer.

$$\Delta G_R^0 \left( \text{J/mole} \right) = \mu_{0,Aq} - \mu_{0,Org} \quad \text{Equation 2}$$

$$\Delta G_R^0 \left( \text{J/mole} \right) = -RT \ln \left( \frac{[REE]_{org}^{eq}}{[REE]_{aq}^{eq}} \right) \quad \text{Equation 3}$$

For the sake of clarity, it should be noted that the reaction Gibbs energy of transfer  $\Delta G_R^0$  standard state is defined for a solvent containing all the species but the rare earth nitrate salt. It is therefore the free energy per mole of transferred species and not the raw difference of a given sample versus a reference state, as classically noted  $\mu^0$  or  $\Delta G^0$  in thermochemistry. There is no assumption considering a dominant supramolecular extraction equilibrium that would take into account all other species present in the solution. The ratio of extracted to remaining species defines the reference free energy linked to the advancement of the reaction. Here, all other species than the one considered are considered part of the solvent and participate in defining the reference state, as explained previously.

One particular interest of this work, is that we performed chemical analysis of both fluids coming out of liquid-liquid extraction device, in order to improve the measurement of the free energy of transfer (See supplementary information 1.4). Indeed, when  $[REE]_{org}$  is well below the standard error of the measurement of  $[REE]_{aq}$ , measuring only  $[REE]_{aq}$  can lead to significant measurement errors on  $[REE]_{org}$ , and hence of both  $[REE]_{org}/[REE]_{aq}$  ratio and Gibbs free energies of transfer (see supplementary information 1.4) Ion concentrations are measured by X-ray fluorescence.

The latter approach differs from most reports available in the literature, that focus on mass balances for which some lack of precision in the measurement of the aqueous residual concentrations of ions left after extraction is acceptable (since efficiency > 90%). In such case, the « remaining » species in the aqueous phase are highly diluted and hence difficult to accurately measure to enable a precise calculation of the ion concentration in the organic phase. To precisely quantify ion concentration of the organic phase, another chemical preparation, such as back extraction, is usually performed prior





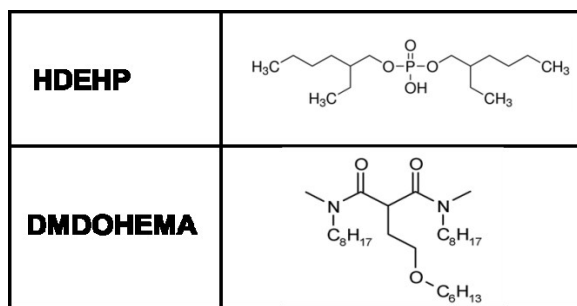


Figure 4: Skeletal formulas of HDEHP and DMDOHEMA.

to capillary chromatography in aqueous medium and quantification via inductively coupled plasma (ICP).

To avoid this and enable accurate measurement of the ratio between extracted and non-extracted ions, an absolute method working for both phases is then needed, such as X-ray fluorescence (XRF).<sup>49</sup> See supplementary information 1.4 for more details on how the calculation of the free energies of transfer from the concentrations of the two phases allows to reduce the errors of measurements by comparing the method used in this study to the classical one i.e measuring aqueous concentrations only.

In this study, the synergic extraction system investigated is composed of the solvating extractant DMDOHEMA and the cation exchanger HDEHP (Figure 4). We selected these as they form a well-studied synergic system based on DMDOHEMA, the latter being known to be efficient to extract lanthanides with high actinides/lanthanides selectivity. More generally DMDOHEMA is a good example of diamine extractants which are known to show high actinides/lanthanide selectivity, a crucial property required when long-lived and short-lived radioactive species coexist in large quantities, such as in closed nuclear cycle that is associated to any fourth generation nuclear plant. Furthermore the viscosity of solutions containing typically 30% of DMDOHEMA in a solvent is acceptable for process design.<sup>50, 51</sup> Moreover, modern predictive approaches exist: (i) to calculate the viscosities observed when solutions are loaded with uranium is available;<sup>52, 53</sup> to derive the critical micellar concentration (cmc) of extractants in different solvents, not only alkanes and solvo-surfactants, but also ionic liquids (such as COSMO-RS).<sup>54</sup>

Overall, our study allows determining the influence of (i) the molar fraction,  $x_{\text{DMDOHEMA}}$ , of the solvating extractant (Equation 4); (ii) the acidity and; (iii) the temperature, on the kinetics, efficiencies and selectivities of the extraction.

$$x_{\text{DMDOHEMA}} = \frac{[\text{DMDOHEMA}]}{[\text{DMDOHEMA}] + [\text{HDEHP}]} \quad \text{Equation 4}$$

In this article, the efficiency is defined as a distribution ratio expressed in standard free energy difference:<sup>55</sup>

$$\Delta G_R^0 \left( \frac{\text{J}}{\text{mole}} \right) = -RT \ln(K_D) \quad \text{Equation 5}$$

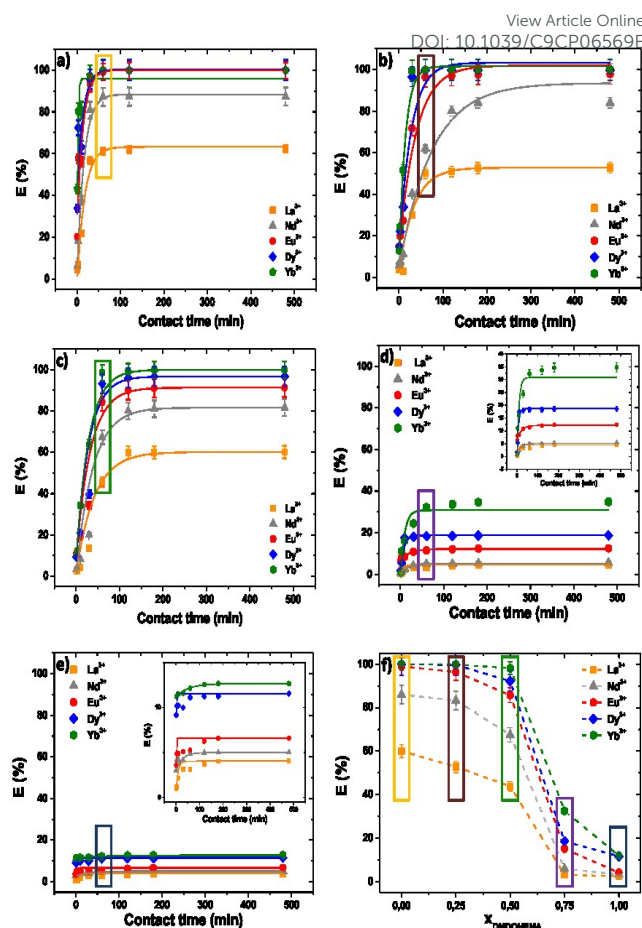


Figure 5: Extraction percentage versus time obtained in microfluidics, with  $[\text{HNO}_3] = 0.03 \text{ M}$ ,  $T = 25^\circ\text{C}$ , for different lanthanides ( $\text{La}^{3+}$ ,  $\text{Nd}^{3+}$ ,  $\text{Eu}^{3+}$ ,  $\text{Dy}^{3+}$ ,  $\text{Yb}^{3+}$ ) and molar fractions,  $x_{\text{DMDOHEMA}} = 0$  (a), 0.25 (b), 0.5 (c), 0.75 (d), 1 (e). (f) Extraction percentages obtained using batch method (1h). Comparing contents of same colour rectangles in graphs (a-e) with the ones in (f) allow visual assessment of reproducibility of microfluidic extraction versus batch extraction measurements (for quantitative data comparisons see Table 1).

Where:

$$K_D = \frac{[\text{REE}]_{\text{org}}}{[\text{REE}]_{\text{aq}}} \quad \text{Equation 6}$$

$K_D$  is the concentration distribution ratio calculated from ionic concentrations in both the organic and aqueous phases after the extraction process.<sup>16</sup>

Note that iron is ten times more concentrated than the rare earths, in order to be representative of typical conditions for recycling of wind-mill magnets.<sup>56</sup> It is an active field of research due to the very large amount of expensive rare earth (neodymium and dysprosium, for example) that can be recycled from them.<sup>57, 58</sup> However, due to (i) overlap of X-ray fluorescence peaks and; (ii) the very low extraction of iron: extracted iron concentrations were too small to be measured either by ICP or XRF. Therefore, we made no tentative of calculating selectivity of the five lanthanides versus iron.





### Comparison of Microfluidic versus Macroscopic Liquid-Liquid Extraction approaches

Various microfluidic approaches to do liquid-liquid extraction have already been proposed, each with advantages and disadvantages, which have already been critically reviewed.<sup>25, 26</sup> To summarize, the main advantages of microfluidic over the batch approach is that most microfluidic platforms enable: (i) a good control and possible variation of the contact time between the two phases (by control of the flow); (ii) a known effective surface of contact. Hence, they enable the quantification of extraction kinetics, otherwise fairly difficult to quantify. More specifically, advantages of the microfluidic platform used in this article are: (i) a large range of contact time can be investigated (which is not the case when the two phases are directly contacted in a co-flow microchannel);<sup>27, 59, 60</sup> (ii) the assembly of the cell and technology required are simple and do not need complex handling / building procedures or expansive process controls such as what is required when using alternating phase droplets.<sup>22</sup> Hence, it should be noted that our simple design and assembly method, using only four screws to hold in place and squeeze the membrane, proved to be very efficient and therefore economical as it enabled us to perform all seventy-five microfluidic extraction experiments, including fifteen membrane exchanges, without any disabling leaking issue. This saves considerable amount of time and effort when compared to non-reversible method of assembly such as gluing or thermal bonding. Importantly, we recently reported that the use of a thin membrane to separate the two phases, such as the one used here, is not a limiting factor, hence it does not modify extraction kinetics.<sup>32</sup>

To compare our microfluidic extraction results with standard approaches, we measured extraction efficiencies for various molar fractions of microfluidic extraction experiments and systematically reproduced these using the macroscopic standard so-called "batch method" in flasks.

From ICP-OES or XRF ion concentration measurements of samples obtained from both organic and aqueous phases using our microfluidic procedure, one can calculate an extraction percentage for each measured data point. The extraction percentage, %E (Equation 7), also called recovery factor, is defined, for any given ion, as the ratio of its concentrations, at equilibrium, in the organic phase  $[REE]_{org}^{out}$  over its concentration in the input aqueous solution  $[REE]_{aq}^{in}$ .

$$\%E = \frac{[REE]_{org}^{out}}{[REE]_{aq}^{in}} \quad \text{Equation 7}$$

Examples of extraction percentages for all studied ions, obtained for various contact times and at 0.03 M in nitric acid, are calculated, plotted and presented in Figure 5. Additional results for other acidities (0.3 and 3 M in  $HNO_3$ ) can be found in supplementary information 1.3). At such acidic concentrations,

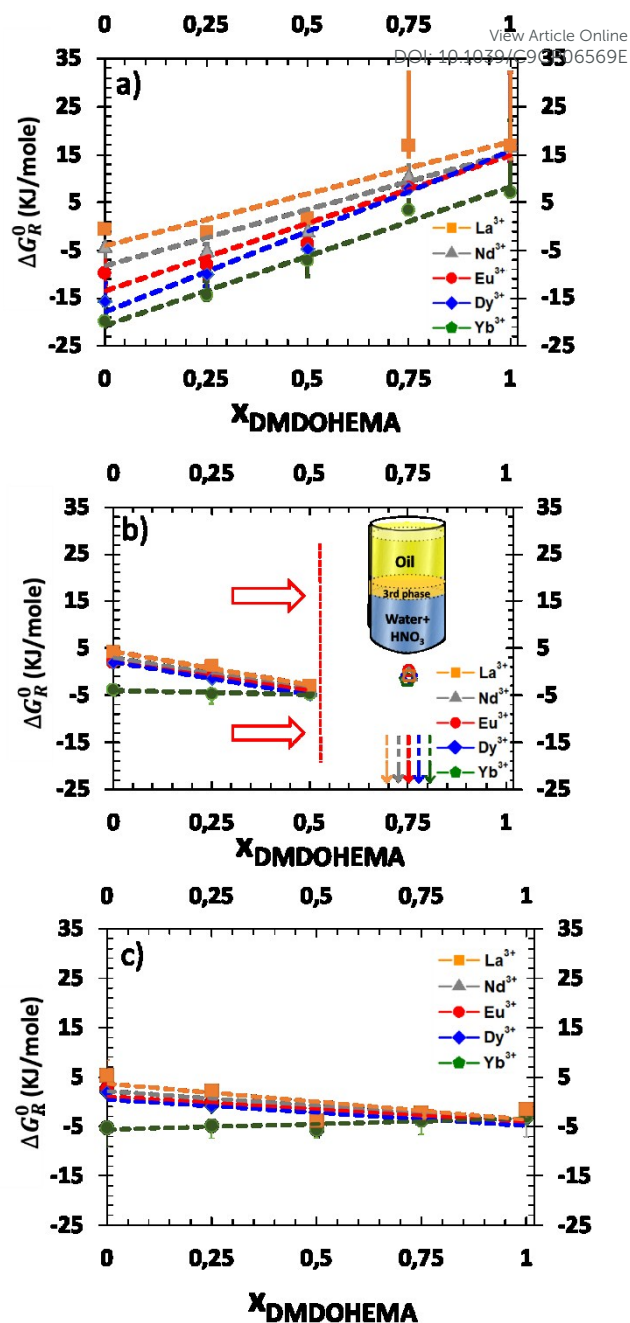


Figure 6: Free energies of transfer  $\Delta G$  (kJ/mole) explored around the Winsor II-Winsor III re-entrant phase limit versus the DMDOHEMA molar fraction for three different  $HNO_3$  concentrations: 0.03 (a), 0.3 (b) and 3M (c).  $T=25^\circ C$ . In b) one can note the observation of a "third phase" when  $x_{DMDOHEMA} > 0.5$  that is observed in the Winsor III domain of the phase diagram. The test tube schematic on the right represents the Winsor III equilibrium: a concentrated "third phase", made of rich extractant structured solution loaded by acid an salts (orange) is formed that coexists at equilibrium with a denser aqueous phase (blue) and a less dense oil rich phase containing diluted extractant monomers, ca. below the CAC (yellow).

pH values are well below 3 where lanthanides and iron ions are trivalent.

Results comparison between microfluidic and batch methods was made for a contact time of 1h. Microfluidic extraction percentages at extraction time identical to standard batch extractions (1h) are highlighted in coloured boxes in Figure 5 (a-e). They can be compared to values obtained using the standard



batch method and given in Figure 5 (f). Quantitatively, the data set acquired both using our microfluidic device and in batch samples for all cations present in solution coincide within experimental uncertainty of the analysis and the difference between the two methods is never more than 3% (See table 1). For example for Ytterbium, this represents at most 0.5 kT ( $\approx 1.2$  kJ/mole) in free energy of transfer.<sup>22</sup>

Table 1: Extraction percentage variation between batch and microfluidics, for different lanthanides ( $\text{La}^{3+}$ ,  $\text{Nd}^{3+}$ ,  $\text{Eu}^{3+}$ ,  $\text{Dy}^{3+}$ ,  $\text{Yb}^{3+}$ ) and  $x_{\text{DMDOHEMA}}$  (0, 0.25, 0.5, 0.75, 1), with  $[\text{HNO}_3] = 0.03$  M,  $T = 25^\circ\text{C}$ .

$x_{\text{DMDOHEMA}}$	La	Nd	Eu	Dy	Yb
0.00	0.0109	0.0116	0.0008	0.0000	0.0000
0.25	0.0270	0.2131	0.0002	0.0003	0.0001
0.50	0.0153	0.0016	0.0151	0.0091	0.0036
0.75	0.0002	0.0094	0.0369	0.0025	0.0028
1.00	0.0063	0.0162	0.0111	0.0057	0.0024

## Study of the Parameters Influencing the Extracting Properties

### Effect of acid concentration:

From Figure 6 (a)-(c) (as well as Figures 1 and 2 of supplementary information) one can estimate that extraction equilibria were reached in times ranging from a few minutes to two hours with the fastest kinetics observed at high acid concentration and the slowest at low acidity (Figure 5 and Supplementary information's Figure 1). This is an additional interest of the microfluidic approach as it directly allows to verify that equilibrium is reached. This is of particular interest when one explore unusual phase diagram domains.

Such influence of the pH on extraction kinetic has previously been explained as being linked to the ion exchange mechanism: at low pH, the concentration of  $\text{H}^+$  in extractant aggregates' polar cores is high which facilitates cation exchange.<sup>20</sup> Although observed curves can show some irregularities, that are likely to be attributed to measurement artefacts, it should be noted that the difference in kinetics for the considered ions could be exploited to enhance selectivity by using contact time that maximise it (and not wait to reach the equilibrium): for example in the absence of DMDOHEMA, fast extraction allows targeting of heavy rare earths. Such observation cannot be obtained using the standard batch approach in the case of fast kinetics. From these, new process protocols of separation and purification could be derived that would work away for the thermodynamic equilibrium.

Furthermore, in order to go beyond a qualitative analysis and enable a more quantitative analysis of the influence of the nitric acid concentration on lanthanides extraction with the mixed system HDEHP and DMDOHEMA, free energies of transfer of lanthanides are measured at various nitric acid concentrations from 0.03 M to 3 M in Isane diluent. Extractions were carried out using same model aqueous phase and with 0.9 M of total

extractant concentration. Results will be discussed and linked to the behaviour of the extractant molecules as well as the electrolyte composition.

Hence, Figure 6 represents the standard-state Gibbs free energy of transfer  $\Delta G_R^0$  (Equation (5)) as a function of the molar fraction of the DMDOHEMA and for three different nitric acid concentrations. For each lanthanide and in the absence of the solvating extractant DMDOHEMA ( $x_{\text{DMDOHEMA}} = 0$ ), one can observe that  $\Delta G_{R, x_{\text{DMDOHEMA}}=0}^0$  values increase significantly when changing  $[\text{HNO}_3]$  from 0.03 (figure 3 in supplementary information and Figure 6(a)) to 0.3 M (Figure 6(b)). Less variations are observed when increasing further  $[\text{HNO}_3]$  (Figure 6 (c)). According to Equation 3, this therefore indicates that  $[\text{REE}]_{\text{org}} / [\text{REE}]_{\text{aq}}$  is decreasing when acidity increases, and thus that the extraction efficiency of lanthanides decreases with the increased acidity and is maximum at  $[\text{HNO}_3] = 0.03$  M.

This has previously been explained as coming from the competition between the transfer of  $\text{H}^+$  from the solvent to aqueous phase and the extraction of lanthanides.<sup>61</sup> More generally, it is often observed when using a cationic exchanger system.<sup>62-64</sup>

The general evolution of the Gibbs free energy  $\Delta G_R^0$  as a function of the molar fractions however differs for each of the three acid concentrations studied. We discuss this behaviour in more details hereafter.

**$[\text{HNO}_3] = 0.03$  M** From a thermodynamic point of view, when the solvating extractant DMDOHEMA molar ratio increases, Figure 6 (a), a linear response in  $\Delta G_R^0$  is observed with a positive slope. This is indicative of a reduction of the extraction toward the organic phase and therefore of an antagonistic effect of DMDOHEMA versus HDEHP appears. This effect has been explained by Ellis *et al.*:<sup>65</sup> trivalent cations are more attracted towards highly negatively charged interface than complexed by solvation only. Indeed, surface charge density is in the order of magnitude of about  $2 \text{ e/nm}^2$  since the area per molecule of HDEHP is typically  $0.5 \text{ nm}^2$  as determined by scattering or surface tension.<sup>66, 67</sup>

**$[\text{HNO}_3] = 0.3$  M** acidity is now increased tenfold when compared to previous paragraph, as shown in Figure 6(b), the curve slopes of  $\Delta G_R^0$  as a function of the molar ratio are negative for all REEs studied with an average value of -8 instead of 25 in the previous case, except for ytterbium. At such an acid concentration in the aqueous phase and above the DMDOHEMA molar fraction of 0.5, we observed the appearance of a dense, viscous third phase.<sup>68</sup> Hence, the oil phase becomes instable at  $x_{\text{DMDOHEMA}} > 0.5$  which prevents the determination of  $\Delta G_R^0$ . Below  $x = 0.5$ , the curves' slopes in Figure 6(b) are significantly reduced by a factor of 3 in absolute value, showing that the intrinsic efficiency of HDEHP is weakened by the large amount of  $\text{H}^+$  competing with rare earths: thus the antagonistic effect of DMDOHEMA disappears.

The two to three phases transition can be understood as a Winsor II to Winsor III equilibria. Winsor II is the coexistence of two fluid phases: a water-poor microemulsion in an oil-continuous medium coexisting with an aqueous phase in excess.<sup>69</sup> Winsor III is a three phases equilibrium. Winsor-II



equilibrium enables standard liquid-liquid extraction processes while entering the Winsor-III domain is a third-phase accident, stopping plants for very long times since all reservoirs must be cleaned. Transition from Winsor II to Winsor III in a liquid-liquid extraction process is due to attraction and coalescence between molecular aggregates producing the splitting of the organic phase into two phases, an extractant-rich and an extractant-poor one, respectively. The latter dilute organic phase has its extractant concentration below the cmc, so all aggregates decompose into monomers.<sup>70</sup> Most Winsor III studied in the literature have been obtained using equal volumes of water and solvent, but they also coexist at low water proportion, even for water volume fractions of less than 10%.<sup>71, 72</sup> Comparing figures 7a, b and c, shows that a Winsor III regime is only observed at intermediate pH, namely  $[\text{HNO}_3] = 0.3 \text{ M}$ . Erlinger *et al.*<sup>68</sup> has already studied similar systems and explain that at low acidity there is not enough extracted species to induce such phase transition by van der Waals forces whereas at high acidity, the coalescence due to interfacial film bending is not strong enough. In classical microemulsions, these are called liquid-liquid phase separation and emulsification failure, respectively.<sup>73, 74</sup>

**$[\text{HNO}_3] = 3 \text{ M}$ :** Results obtained are plotted in Figure 6(c) as well as in an enlarged scale for each ion in Figure 7(a-e). Most curves of  $\Delta G_R^0$  versus molar fraction exhibits a nonlinear synergic behaviour, ca. the free energy of transfer measured is lower than the value that would be expected from a linear interpolation between the  $\Delta G_R^0$  values for each of the two molecules when present alone in the solution. This interpolation is also represented together with their fitting curves using a quadratic function Figure 7(a-e).<sup>75</sup> It should be noted that the molar fraction of the mixture for which the synergy is maximum is always measured close to the molar fraction  $x_{\text{DMDOHEMA}} = 0.5$ , similarly to previous report by Bley *et al.*<sup>48</sup>

Table 2: experimental entropy coefficients deduced from fits.

Ion	La <sup>3+</sup>	Nd <sup>3+</sup>	Eu <sup>3+</sup>	Dy <sup>3+</sup>	Yb <sup>3+</sup>
Entropy coefficient (A)	7.1	6.2	6.3	5.5	1.5

As recently detailed by Spadina *et al.*, the free energy of transfer can be expressed as the sum of different terms: (i) complexation term; (ii) bulk term which represents the reduction of accessible volume solutes confinement in cores of aggregates and; (iii) other electrostatic terms.<sup>76</sup> This is also valid in the case of mixed micelles with two extracting molecules.<sup>76</sup> In this latter case, according to Spadina *et al.*, the sum of the entropic part of these three terms seems to be dominant which enhanced synergy extraction as due to the increase of configurational entropy for extracted ions.

The configurational mixing entropy inside the aggregate formed by the extractant in first and second coordination spheres<sup>77</sup> can be expressed as follow:<sup>75, 78-80</sup>

$$\Delta S = A \cdot k \cdot T \cdot x(1-x) \quad \text{Equation 8}$$

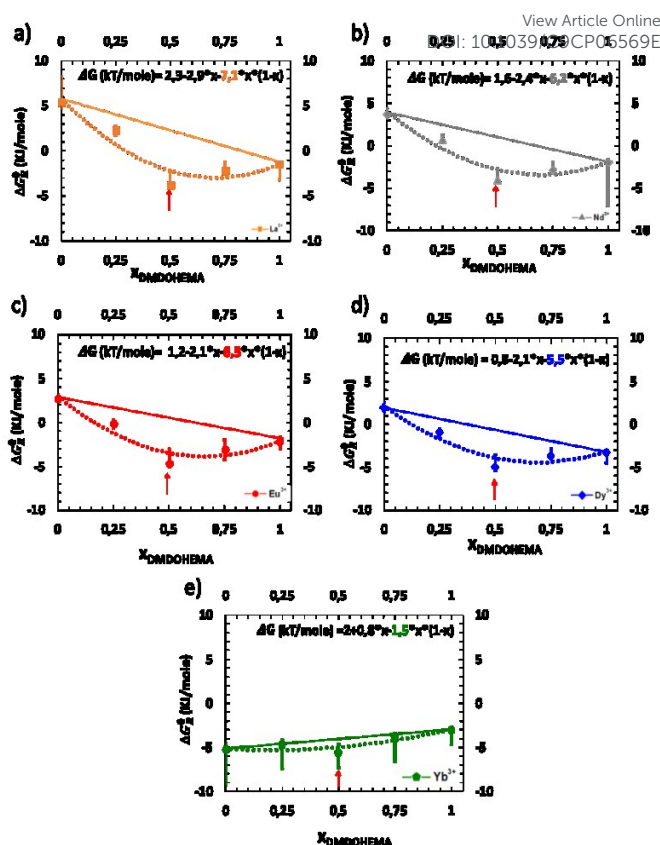


Figure 7: graphical representation of the efficiency of extraction (expressed in step of chemical potential (kJ/mole)) for different lanthanides from a highly concentrated nitric acid solution in Winsor II equilibrium with a solvent phase containing a mixture of DMDOHEMA and HDEHP at constant total extractant concentration of 0.9M. Initial aqueous phase:  $[\text{Ln(III)}] = 10 \text{ mM}$ ,  $[\text{HNO}_3] = 3 \text{ M}$ ,  $T = 25^\circ\text{C}$ . The red arrows stand for the molar fraction where synergism reaches its maximum: a) La<sup>3+</sup>; b) Nd<sup>3+</sup>; c) Eu<sup>3+</sup>; d) Dy<sup>3+</sup>; e) Yb<sup>3+</sup>.

Where the prefactor A depends on the exact number molecules in the first and second molecular spheres around extracted ions. For this reason, it is useful to plot free energies of transfer versus molar fractions as it quickly gives an indication of the number of degrees of freedom involved. Numerical values

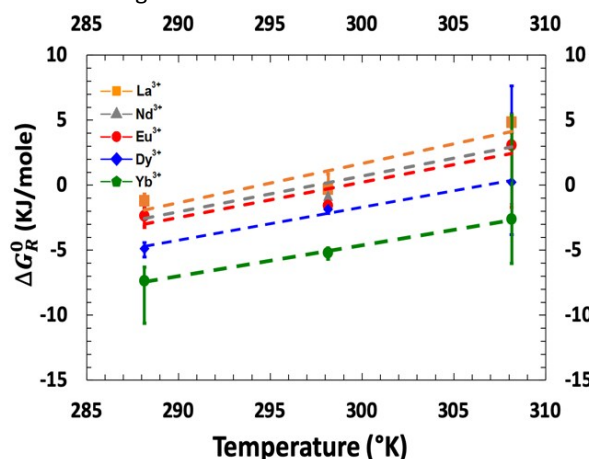


Figure 8: Evolution of the free energy of transfer as a function of the temperature for the five lanthanides and for a total extractant concentration of 0.9 M (50% DMDOHEMA) in Isane.

corresponding to this factorization (A) are calculated from the





fits in the Figure 7(a)-(e) and indicated explicitly in the Table 2. Most experimental values for the entropy coefficient A are between five and six.

Such excess in configuration entropy can be associated with the many possible arrangements of the ion in the polar core of the aggregate, which is intrinsically included in molecular dynamics, but neglected in quantum chemistry (second coordination sphere).<sup>76</sup> Hence, since in that case (i) synergy is reported to be mostly due to configurational entropy and not to a specific unique stoichiometry of defined complexes as used in parametric model<sup>30</sup> and; (ii) we assume that the main contribution to entropy is due to the extractant present in the aggregate and not to co-extracted nitric acid or water, then we can evaluate the configuration excess mixing entropic according to:<sup>33, 75</sup>

$$\Delta S(J/mole) = RT \ln \left( \frac{(N_c + N_s)!}{N_c! N_s!} \right) \quad \text{Equation 9}$$

Considering, (i) the expression of the extractants entropy given in Equation 9 and (ii) the hypothesis that aggregates are made of about ten interacting molecules of both solvating extractants ( $N_s$ ) and charged surfactants ( $N_c$ ):  $N_s + N_c = 10$ , one can tabulate the entropy as a function of the number of charged surfactants per aggregate (Table 3). N.B. we assumed that number since, according to reference<sup>81</sup>, most efficient extraction systems have local water in oil cylindrical microstructure, with both a typical cylinder diameter and length per extracted ion in the order of one nanometre. From this, the number of complexing molecules in first and second coordination position can easily be calculated to be between eight and ten. From Table 3, expected values for the entropy should be between 2 and 5 and furthermore, one can also observe that it is maximum for  $N_c=5$ , similarly to the experimentally determined synergy which is also maximum for a molar ratio of 0.5.

Since entropy experimental values, listed in Table 2 (ranging between 1.5 and 7 for Ytterbium and Lanthanum, respectively), and the calculated ones are of a similar order of magnitude, this is coherent with the fact that surface excess mixing entropy is the dominant term responsible of the synergy effect.<sup>76</sup> Further mechanism studies of surface mixing entropy are however yet required to explain the variability of synergy versus ionic radius of the lanthanides.

Table 3: Entropy estimates in the extracting molecules aggregates as a function of the number of charged surfactants, calculated using equation 9.

$N_c$	1	2	3	4	5	6	7
$\Delta S_{cal}$	2.3	3.8	4.78	5.34	5.6	5.3	4.78

Results presented and fitted in Figure 7 and discussed above demonstrate also the interest of precise measurement of  $\Delta G_R^0$  as a function of the molar fraction. Indeed, we just showed that it enables the estimation of the extracting aggregates' composition for which a drastic enhancement of separation

efficiency is observed. Indeed, in the case of Dysprosium (Figure 7d), at a molar fraction of 0.5, one can measure a Synergic Gibbs free energy variation, written  $\Delta \Delta G_R^0$ , which is the difference between the experimental Gibbs free energy measured with the one calculated from linear interpolation at  $x = 0.5$ , see Figure 7. In the latter case,  $\Delta \Delta G_R^0$  is equal to 4. This means that the extraction efficiency is improved by almost two orders of magnitude ( $\times 50$ ).

### Effect of temperature

The Gibbs free energies of transfer for the five lanthanides were determined for three different temperatures ranging from 15°C to 35°C, with  $[HNO_3] = 3 \text{ mol}\cdot\text{L}^{-1}$ , DMDHEMA's molar fraction of 0.5 and a total amount of extractants of 0.9 M. Plotted results are presented in Figure 8 and precise values for each data point are given in supplementary information. The increasing of the free energy of transfer with the temperature indicates an exothermic nature of the extraction process (Figure 8).

According to the literature, all lanthanide extraction by amides or mixed extractants are enthalpy driven,<sup>48, 82, 83</sup> with yet unpredictable effects of solvent branching or monomer isomerisation.<sup>84</sup> In classical thermodynamics and when considering the extraction process as a whole, the standard van't Hoff derivation used for simple fluids can be used only when (i) all aggregation effects are negligible and (ii) enthalpy itself has no temperature dependence. With these two restrictions, all entropy variations can be calculated from the derivatives of the free energy with respect to the temperature. It should be noted that this van't Hoff approach is only valid for ideal fluids, it is not numerically correct and no more valid when aggregation or electrostatic effects are more than 2-5 kJ/mole. If we suppose that configurational mixing entropy of the extraction is much larger than other contributions such as complexation entropy, then we can consider as in classical thermodynamics. Considering the linear dependence of the Gibbs free energies of transfer of lanthanides versus temperature (Equation 10), the plot of  $\Delta G_R^0$  as a function of temperature leads to a straight line from which: (i) the entropy of complexation ( $\Delta S^0$ ) can be measured directly as its slope and; (ii) the enthalpy of complexation ( $\Delta H^0$ ) is equal to the intercept values.

$$\Delta G^0 = \Delta H^0 - T\Delta S^0 \quad \text{Equation 10}$$

where  $\Delta H^0$  and respectively  $\Delta S^0$  are the enthalpic and entropic parts, respectively, of all coexisting extraction mechanisms. Negative values measured for  $\Delta H$  indicate the exothermic nature of the extraction process. Furthermore, one can observe that all slopes are positive (measured  $\Delta S^0$  are given in Table 4). Since strong slopes are indicative of strong entropic contributions to the extraction process (Figure 8, Table 4), this is coherent with extraction efficiencies maximum at the lowest temperature values accessible experimentally.

Table 4: values of measured  $\Delta S^0$

ION	La <sup>3+</sup>	Nd <sup>3+</sup>	Eu <sup>3+</sup>	Dy <sup>3+</sup>	Yb <sup>3+</sup>
$\Delta S^0_{measured} (J/mol)$	-302	-274	-271	-254	-237





As said before, one must however be careful when using this approach<sup>85</sup> as it only applies when the solvent's structuration is independent of the temperature. Nevertheless, it allowed us to determine quantitatively averaged thermodynamic parameters. All measured averaged thermodynamic parameters  $\Delta S^0$  and  $\Delta H^0$  for extraction are given in supplementary information and plotted in Figure 9 versus various characteristics of the considered REEs.

From these measured values and for all lanthanides tested here, it has been found that REE extractions are mainly driven by strong enthalpies of complexation, although they are also

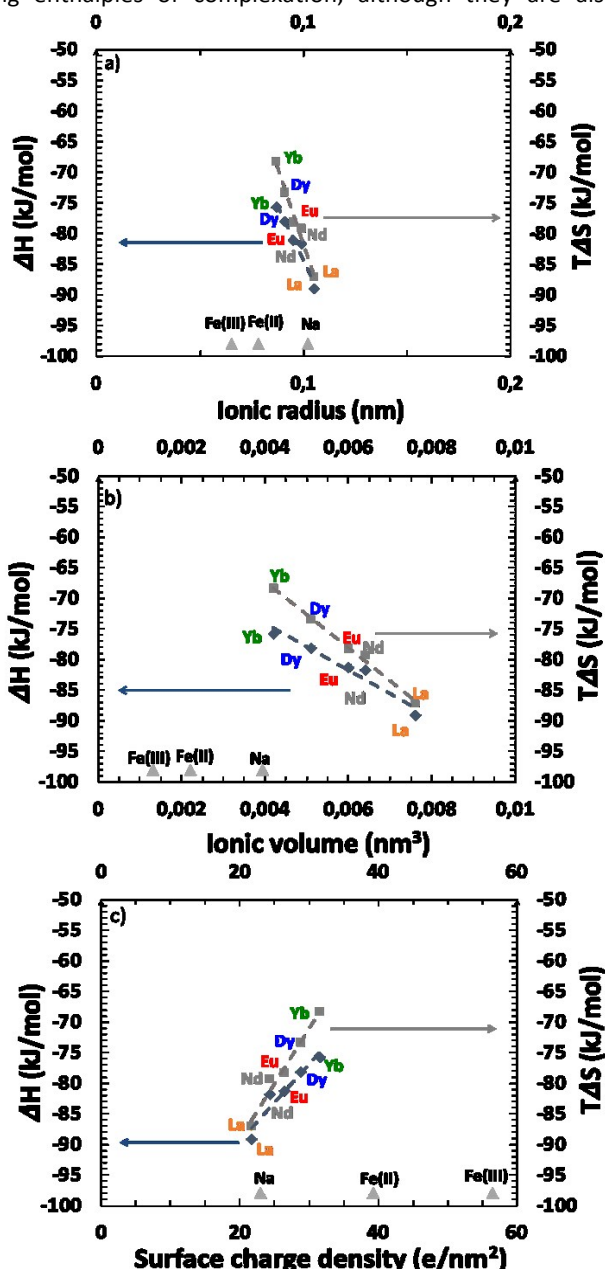


Figure 9: Entropy-Enthalpy compensation for the different lanthanides tested expressed versus three physical quantities: (a) radius as used in structural studies, (b) volume that is important for all depletion effect and (c) surface charge density as used to evaluate electrostatic contribution.

associated to negative entropy terms, which favours the initial state in water. A higher exothermic enthalpy value ( $-\Delta H^0$ ) for lanthanum suggests its stronger binding with the mixed system compared to dysprosium for example. The negative entropy change ( $\Delta S^0$ ) may be associated with a loss of translation and rotation entropy of the mixed extractant system during complexation in the volume of the extracted species.

The Yb (III) -DMDOHEMA / HDEHP complex seems to be more favourable than the La (III) - DMDOHEMA / HDEHP one, since  $-\Delta G^0$  for ytterbium is larger than that for lanthanum.

If we compare behaviours within the lanthanides family, three quantities are typically discussed regarding the origin of selectivity:<sup>86</sup> ionic radius (Figure 9a), ionic volume (Figure 9b) and surface charge density (Figure 9c). All plots are linear for enthalpy as well as entropy so the dominant mechanism cannot be directly determined from these plots. The effect of surface charge density shown in Figure 9c, leads to larger extraction of lanthanides versus iron. Since the charge effect seems to be little, this indicates that non-electrostatic complexation is dominant but it is not the only important effect, since complexation also follows Pearsons HSAB principle.<sup>87-90</sup>

In any case, one of the core property of the ieanics approach is that the speciation of the different complexes in the water phase is not needed in order to interpret the free energy of transfer of the solute. Moreover, the ieanics approach does not suppose any "dominant" reaction: it considers the energy of the transfer in the presence of a large number of polydisperse W/O aggregates coexisting. There are therefore hundreds of competing equilibria between weak aggregates and there is no reason to presuppose the existence of a single stoichiometric "reaction mechanism" similarly to monodisperse "complexes" that are sometimes co-crystallize with water and salts.<sup>32, 61, 68</sup>

#### Additional findings

The microfluidic set-up was designed for the study of phase diagrams in the Winsor II regime allowing efficient extraction and stripping. Surprisingly, our result indicates that the Winsor III<sup>16, 68, 91, 92</sup> regime could also be obtained, although in the collecting tube of the solvent phase. This liquid-liquid instability of the solvent phase occurs therefore spontaneously and without the need of mixing and emulsification. The top phase is nearly pure solvent and contains only extractant monomers. The latter coexists with the third phase. Even without gentle centrifugation, it was possible to take a sample for analysis with a syringe. Due to the unique dynamic range of XRF, as well as the absence of further preparation, the dosage of both the diluted and the concentrated optically birefringent mesophase of condensed aggregate could be performed. It should be noted that the phase separation was not visible by naked eye in the



channels of the microfluidic device. Its occurrence was also cross-checked with the batch method where, after extraction, the extractant-rich and extractant-poor phases could be collected separately and our XRF analysis protocol used. Hence, in this regime, the free energy of transfer could even be obtained in the diluted phase, for the first time to our best knowledge.

Figure 6b illustrates the case where the acid concentration is equal to 0.3 M but for molar fractions of DMDOHEMA strictly greater than 0.5 and where a concentrated "third phase" is formed which coexists with a diluted organic solution as Winsor III equilibria.<sup>14, 68, 93</sup> Figure 10 present observed free energies of transfer for the diluted phase (light yellow), that are ranging between  $\sim -0.5$  to  $-1.5$  kJ/mole. Regarding the third phase (orange), made from interconnected polar cylinders,<sup>81</sup> Gibbs free energy are too strong to be measured with ions concentrations in the organic phase that are too low (hence free energies of transfer values diverge, which we represented with arrows pointing down going all the way).

We assembled graphically the main findings of this work in a schematic form in Figure 10, including free energies of transfer of the Winsor III diluted phase. Ions exchanges occur between aqueous (in blue) and solvent-rich phases (orange and light yellow). Kinetic barrier and asymmetry in the transfer rate are due to the thin interfacial domain, also called interphase,<sup>23</sup> that

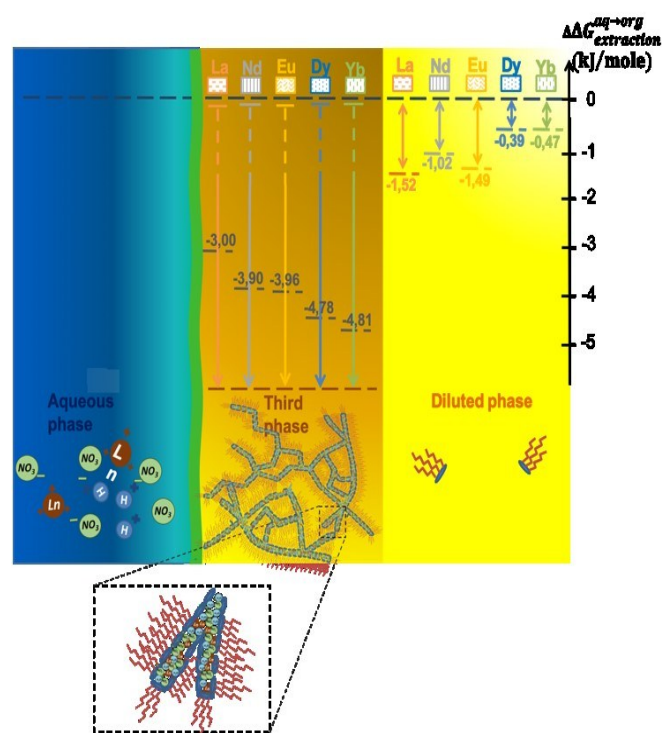


Figure 10: Relation between the driving force for extraction observed in three different cases: bold black dashed levels represents best measured extraction efficiencies (see equation. 5) in the Winsor II equilibria situated at the limit of the phase ( $[HNO_3] = 0.3$  M,  $x_{DMDOHEMA} = 0.25$ ); for the third condensed phase made from interconnected polar cylinders, the chemical potential step is too large to be measured (hence the infinite arrows); in the diluted phase, free energy steps are small but measurable (coloured dotted lines).

is schematized as a green line.<sup>94,95</sup> Again, in the diluted phase, complexation versus entropy balance results in low but

measurable energy of transfer.<sup>78, 79</sup> Moreover, as previously reported,<sup>34</sup> the domain where extraction is most efficient and optimum for liquid-liquid formulation in industrial plant feed is close to the third phase appearance point.

## Conclusions

In this report, after presenting a simple although versatile microfluidic assembly enabling the study of liquid-liquid extraction, we then report its use for the study of a synergetic extracting system hereby enabling:

- the acquisition of kinetics data, otherwise difficult to obtain using standard batch method or other more complex microfluidic systems;
- to study the influence of acid concentration, molar fraction and temperature, thus giving access to pieces of information on the stoichiometry of the aggregate forming in organic solvent;
- to prove the interest of measuring the concentrations in both aqueous and organic phases by a constrained fit which increases result's precision down to 2 kJ/mole (1kT/molecule) (see supporting information 1.4);
- the simultaneous study of multiple chemical elements solution and therefore of realistic model or real lixiviates;
- to greatly reduce the amount of chemicals used for such a study (only 10.86 g of DMDOHEMA, 7.25 g of HDEHP and 73 mL of Isane/water were used in total here. This could further be reduced by about one order of magnitude with on-line XRF).

Finally, it appears that this device is also adapted in the case when the solvent channels is the locus of a phase separation. Thus this device could also be used for the collection and study of the Winsor III equilibria. Although, if in the classical extraction regime (Winsor II), we have shown in a previous paper that the chosen membrane is not a limiting factor,<sup>32</sup> it has recently been evidenced that liquid-liquid and liquid-solid interfaces increase the domain of stability of the liquid crystals that constitute the "third phase".<sup>23</sup> Therefore, results concerning experiments where a third phase may be present in the pores of the membrane will have to be considered with care and with some uncertainty regarding the exact composition of the final equilibrium state.

Once fully integrated with computer controlled mixing capability and online characterization methods such as hollow waveguide FTIR,<sup>24, 96</sup> and XRF,<sup>31</sup> and ultimately small angle X-ray scattering, we anticipate that phase diagram exploration can be fully automatized, with very little down time. It would furthermore also give access to kinetics information, otherwise difficult to obtain. Ultimately, a two stages system would allow studying simultaneously both extraction and desextraction, as well as the recycling of the organic extractant. Hence such tools should accelerate the study of liquid-liquid extraction processes, a key factor to enable the recycling of highly variable waste streams lixiviates.



## Conflicts of interest

There are no conflicts to declare.

## Acknowledgements

All authors would like to pay our gratitude Helmuth Möhwald, who passed away in March 2018, for helpful scientific discussions and counselling, as well as Sandrine Dourdain, Jean-François Dufrêche and Stéphane Pellet-Rostaing (CEA/DRF/ICSM) for help in CP's initial training in batch extraction and consortium meeting discussions. AEM, JT, CP and JCG would like to thank Frédéric Né, Nicolas Verplanck, François Boizot and Manuel Alessio at CEA/DRT/LETI for help with microfluidics manufacturing, as well as final year intern Gabriel Bernard for incremental improvement of the microfluidic platform (design & implementation of the counter pressure control, and syringe pump modification) and preliminary extraction testing. All experimental research leading to these results was performed at CEA and received funding from the European Research Council under the European Union's 7<sup>th</sup> Framework Program (FP/2007-2013)/ERC Grant Agreement N° [320915] "REE-CYCLE": Rare Earth Element reCYCling with Low harmful Emissions.

## Notes and references

1. Z. Sun, H. Cao, Y. Xiao, J. Sietsma, W. Jin, H. Agterhuis and Y. Yang, *Acs Sustainable Chemistry & Engineering*, 2017, **5**, 21-40.
2. S. Glozier, L. T. Espinoza, C. Gandenberger and M. Faulstich, *Resources Policy*, 2015, **44**, 35-46.
3. T. Cheisson and E. J. Schelter, *Science*, 2019, **363**, 489-493.
4. J. Lucas, P. Lucas, T. Le Mercier, A. Rollat, W. Davenport, J. Lucas, P. Lucas, T. LeMercier, A. Rollat and W. Davenport, *Rare Earth Production, Use and Price*, 2015.
5. C. Tunsu, M. Petranikova, M. Gergoric, C. Ekberg and T. Retegan, *Hydrometallurgy*, 2015, **156**, 239-258.
6. W. J. Albery and R. A. Choudhery, *Journal of Physical Chemistry*, 1988, **92**, 1142-1151.
7. N. Urasaki, C. P. Wong, Ieee and Ieee, *Separation of low molecular siloxanes for electronic application by liquid-liquid extraction*, 1999.
8. K. Binnemans, P. T. Jones, B. Blanpain, T. Van Gerven, Y. Yang, A. Walton and M. Buchert, *Journal of Cleaner Production*, 2013, **51**, 1-22.
9. J. Lucas, P. Lucas, T. L. Mercier, A. Rollat and W. G. Davenport, *Rare Earths, 1st edition*, Elsevier, first edn., 2014.
10. H. S. Yoon, C. J. Kim, K. W. Chung, S. D. Kim, J. Y. Lee and J. R. Kumar, *Hydrometallurgy*, 2016, **165**, 27-43.
11. A. M. Wilson, P. J. Bailey, P. A. Tasker, J. R. Turkington, R. A. Grant and J. B. Love, *Chem. Soc. Rev.*, 2014, **43**, 123-134.
12. J. Veliscek-Carolan, *Journal of Hazardous Materials*, 2016, **318**, 266-281.
13. H. F. Eicke and H. Christen, *Helvetica Chimica Acta*, 1978, **61**, 2258-2263.
14. C. Bauer, P. Bauduin, J. F. Dufreche, T. Zemb and O. Diat, *European Physical Journal Special Topics*, 2012, **213**, 225-241.
15. G. Gompper and M. Schick, in *Phase transitions and critical phenomena. Self-assembling amphiphilic systems*, vol. 16, Academic Press, London, 1994, pp. 1-181.
16. T. Zemb, C. Bauer, P. Bauduin, L. Belloni, C. Dejumat, O. Diat, V. Dubois, J. F. Dufreche, S. Dourdain, M. Duvail, C. Larpent, F. Testard and S. Pellet-Rostaing, *Colloid and Polymer Science*, 2015, **293**, 1-22.
17. R. J. Ellis, Y. Meridiano, J. Muller, L. Berthon, P. Guilbaud, N. Zorz, M. R. Antonio, T. Demars and T. Zemb, *Chemistry-a European Journal*, 2014, **20**, 12796-12807.
18. R. J. Ellis, Y. Meridiano, R. Chiarizia, L. Berthon, J. Muller, L. Couston and M. R. Antonio, *Chemistry-a European Journal*, 2013, **19**, 2663-2675.
19. B. F. Qiao, J. V. Muntean, M. O. de la Cruz and R. J. Ellis, *Langmuir*, 2017, **33**, 6135-6142.
20. M. Špadina, K. Bohinc, T. Zemb and J.-F. Dufrêche, *Langmuir*, 2018, **34**, 10434-10447.
21. R. Motokawa, T. Kobayashi, H. Endo, J. J. Mu, C. D. Williams, A. J. Masters, M. R. Antonio, W. T. Heller and M. Nagao, *ACS Central Sci.*, 2019, **5**, 85-96.
22. K. P. Nichols, R. R. Pompano, L. Li, A. V. Gelis and R. F. Ismagilov, *Journal of the American Chemical Society*, 2011, **133**, 15721-15729.
23. M. Corti, A. Raudino, L. Cantu', J. Theisen, M. Pleines and T. Zemb, *Langmuir*, 2018, **34**, 8154-8162.
24. V. Kokoric, J. Theisen, A. Wilk, C. Penisson, G. Bernard, B. Mizaikoff and J. C. P. Gabriel, *Analytical Chemistry*, 2018, **90**, 4445-4451.
25. D. Ciceri, J. M. Perera and G. W. Stevens, *J. Chem. Technol. Biotechnol.*, 2014, **89**, 771-786.
26. C. Xu and T. L. Xie, *Industrial & Engineering Chemistry Research*, 2017, **56**, 7593-7622.
27. G. Hellé, C. Mariet and G. Cote, *Procedia Chemistry*, 2012, **7**, 679-684.
28. D. Mark, S. Haeberle, G. Roth, F. von Stetten and R. Zengerle, *Chem. Soc. Rev.*, 2010, **39**, 1153-1182.
29. G. M. Whitesides, *Nature*, 2006, **442**, 368-373.
30. M. Tokeshi and T. Kitamori, in *Handbook of capillary and microchip electrophoresis and associated microtechniques*, ed. J. P. Landers, Taylor & Francis, Boca Raton, Third edn., 2007, DOI: <https://doi.org/10.1201/9781420004953>, ch. 35, pp. 1021-1036.
31. C. Penisson, Ph. D., Université de Grenoble Alpes, 2018.
32. J. Theisen, C. Penisson, J. Rey, T. Zemb, J. Duhamet and J. C. P. Gabriel, *J. Membr. Sci.*, 2019, **586**, 318-325.
33. J. Rey, S. Dourdain, J.-F. Dufrêche, L. Berthon, J. M. Muller, S. Pellet-Rostaing and T. Zemb, *Langmuir*, 2016, **32**, 13095-13105.
34. J. Rydberg, M. Cox, C. Musikas and C. G. R., eds., *Solvent Extraction Principles and Practice, Revised and Expanded*, Marcel Dekker Inc., New York, 2004.
35. B. Abecassis, F. Testard, T. Zemb, L. Berthon and C. Madic, *Langmuir*, 2003, **19**, 6638-6644.





36. L. Berthon, L. Martinet, F. Testard, C. Madic and T. Zemb, *Solvent Extraction and Ion Exchange*, 2007, **25**, 545-576.
37. G. Helle, C. Mariet and G. Cote, *Talanta*, 2015, **139**, 123-131.
38. H. F. Eicke, *Topics in current chemistry*, 87, pp. 85-145, 1980.
39. J. M. Muller, C. Berthon, L. Couston, D. Guillaumont, R. J. Ellis, N. Zorz, J. P. Simonin and L. Berthon, *Hydrometallurgy*, 2017, **169**, 542-551.
40. J. Rey, S. Atak, S. Dourdain, G. Arrachart, L. Berthon and S. Pellet-Rostaing, *Solvent Extraction and Ion Exchange*, 2017, **35**, 321-331.
41. S. Dourdain, I. Hofmeister, O. Pecheur, J. F. Dufreche, R. Turgis, A. Leydier, J. Jestin, F. Testard, S. Pellet-Rostaing and T. Zemb, *Langmuir*, 2012, **28**, 11319-11328.
42. J. Muller, PhD Thesis, Université Pierre et Marie Curie-Paris VI, 2012.
43. G. J. Lumetta, A. V. Gelis and G. F. Vandegrift, *Solvent Extraction and Ion Exchange*, 2010, **28**, 287-312.
44. P. Bauduin, F. Testard and T. Zemb, *Journal of Physical Chemistry B*, 2008, **112**, 12354-12360.
45. A. V. Gelis and G. J. Lumetta, *Industrial & Engineering Chemistry Research*, 2014, **53**, 1624-1631.
46. M. K. Jha, A. Kumari, R. Panda, J. R. Kumar, K. Yoo and J. Y. Lee, *Hydrometallurgy*, 2016, **165**, 2-26.
47. T. Zemb, M. Duvail and J. F. Dufreche, *Israel Journal of Chemistry*, 2013, **53**, 108-112.
48. J. Rey, M. Bley, J.-F. Dufrêche, S. Gourdin, S. Pellet-Rostaing, T. Zemb and S. Dourdain, *Langmuir*, 2017, **33**, 13168-13179.
49. S. E. Mann, M. C. Ringo, G. Shea-McCarthy, J. Penner-Hahn and C. E. Evans, *Anal Chem*, 2000, **72**, 1754-1758.
50. M. Duvail, T. Dumas, A. Paquet, A. Coste, L. Berthon and P. Guilbaud, *Physical Chemistry Chemical Physics*, 2019, **21**, 7894-7906.
51. R. Malmbeck, D. Magnusson, S. Bourg, M. Carrott, A. Geist, X. Heres, M. Miguiditchian, G. Modolo, U. Mullich, C. Sorel, R. Taylor and A. Wilden, *Radiochimica Acta*, 2019, **107**, 917-929.
52. M. Pleines, W. Kunz, T. Zemb, D. Benczedi and W. Fieber, *Journal of Colloid and Interface Science*, 2019, **537**, 682-693.
53. M. Pleines, W. Kunz and T. Zemb, *Journal of Surfactants and Detergents*, 2019, **22**, 1011-1021.
54. M. Grabda, M. Panigrahi, S. Oleszek, D. Kozak, F. Eckert, E. Shibata and T. Nakamura, *Fluid Phase Equilib.*, 2014, **383**, 134-143.
55. B. Moeser and D. Horinek, *Biophysical Chemistry*, 2015, **196**, 68-76.
56. T. Zemb and J.-C. P. Gabriel, *Final Report Summary ERC 320915: REE-CYCLE (Rare Earth Element reCYCLing with Low harmful Emissions)* European Union 2019.
57. Y. X. Yang, A. Walton, R. Sheridan, K. Guth, R. Gauss, O. Gutfleisch, M. Buchert, B. M. Steenari, T. Van Gerven, P. T. Jones and K. Binnemans, *Journal of Sustainable Metallurgy*, 2017, **3**, 122-149.
58. M. Panigrahi, M. Grabda, D. Kozak, A. Dorai, E. Shibata, J. Kawamura and T. Nakamura, *Sep. Purif. Technol.*, 2016, **171**, 263-269.
59. Y. Kikutani, K. Mawatari, A. Hibara and T. Kitamori, *Microchimica Acta*, 2008, **164**, 2411-2417. [View Article Online](#) DOI: 10.1002/C9CP06569E
60. X. Wang, C. Saridara and S. Mitra, *Analytica Chimica Acta*, 2005, **543**, 92-98.
61. C. Dejognat, S. Dourdain, V. Dubois, L. Berthon, S. Pellet-Rostaing, J. F. Dufreche and T. Zemb, *Physical Chemistry Chemical Physics*, 2014, **16**, 7339-7349.
62. A. E. Visser, R. P. Swatloski, S. T. Griffin, D. H. Hartman and R. D. Rogers, *Separation Science and Technology*, 2001, **36**, 785-804.
63. A. Rout, J. Kotlarska, W. Dehaen and K. Binnemans, *Physical Chemistry Chemical Physics*, 2013, **15**, 16533-16541.
64. D. F. Peppard, G. W. Mason, J. L. Maier and W. J. Driscoll, *Journal of Inorganic & Nuclear Chemistry*, 1957, **4**, 334-343.
65. R. J. Ellis, T. Demars, G. Liu, J. Niklas, O. G. Poluektov and I. A. Shkrob, *Journal of Physical Chemistry B*, 2015, **119**, 11910-11927.
66. D. C. Steytler, D. L. Sargeant, G. E. Welsh, B. H. Robinson and R. K. Heenan, *Langmuir*, 1996, **12**, 5312-5318.
67. D. C. Steytler, T. R. Jenta, B. H. Robinson, J. Eastoe and R. K. Heenan, *Langmuir*, 1996, **12**, 1483-1489.
68. C. Erlinger, L. Belloni, T. Zemb and C. Madic, *Langmuir*, 1999, **15**, 2290-2300.
69. S. A. Safran and L. A. Turkevich, *Physical Review Letters*, 1983, **50**, 1930-1933.
70. S. Prevost, M. Gradzielski and T. Zemb, *Advances in Colloid and Interface Science*, 2017, **247**, 374-396.
71. K. Osseo-Asare, *Advances in Colloid and Interface Science*, 1991, **37**, 123-173.
72. M. Duvail, L. Arleth, T. Zemb and J. F. Dufreche, *Journal of Chemical Physics*, 2014, **140**.
73. A. Jada, J. Lang, S.-J. Candau and R. Zana, *Colloids and Surfaces*, 1989, **38**, 251-261.
74. A. Jada, J. Lang and R. Zana, *Journal of Physical Chemistry*, 1990, **94**, 381-387.
75. K. A. Dill and S. Bromberg, *Molecular driving forces*, Garland Science ; Taylor & Francis [distributor], New York; London, 2010.
76. M. Špadina, K. Bohinc, T. Zemb and J.-F. Dufrêche, *ACS Nano*, 2019, DOI: 10.1021/acsnano.9b07605.
77. J. Rey, S. Dourdain, L. Berthon, J. Jestin, S. Pellet-Rostaing and T. Zemb, *Langmuir*, 2015, **31**, 7006-7015.
78. L. Sapir and D. Harries, *Current Opinion in Colloid & Interface Science*, 2015, **20**, 3-10.
79. L. Sapir and D. Harries, *Current Opinion in Colloid & Interface Science*, 2016, **22**, 80-87.
80. S. Sukenik, L. Sapir and D. Harries, *Current Opinion in Colloid & Interface Science*, 2013, **18**, 495-501.
81. P. Guilbaud, L. Berthon, W. Louisfremat, O. Diat and N. Zorz, *Chemistry-a European Journal*, 2017, **23**, 16660-16670.
82. S. Vafaei, B. Tomberli and C. G. Gray, *Journal of Chemical Physics*, 2014, **141**.
83. H. Singh, S. L. Mishra and R. Vijayalakshmi, *Hydrometallurgy*, 2004, **73**, 63-70.
84. M. S. Tyumentsev, M. R. S. J. Foreman, B.-M. Steenari and C. Ekberg, *The Journal of Chemical Thermodynamics*, 2019, **131**, 133-148.





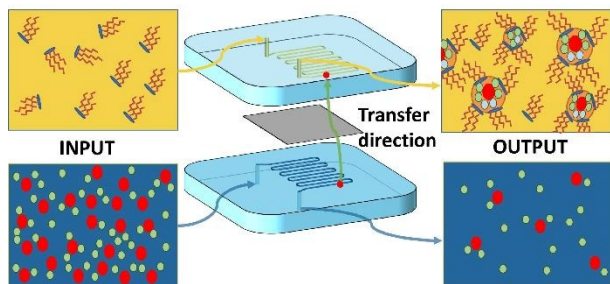
85. M. S. Tyumentsev, M. R. S. Foreman, B. M. Steenari and C. Ekberg, *Journal of Chemical Thermodynamics*, 2019, **131**, 133-148.
86. Y. Marcus, *Ions in Solution and their Solvation*, John Wiley & Sons Inc. , Hoboken, Nex Jersey, 2015.
87. R. D. Hancock and A. E. Martell, *Chemical Reviews*, 1989, **89**, 1875-1914.
88. R. G. Pearson, *Journal of the American Chemical Society*, 1963, **85**, 3533-3539.
89. R. G. Pearson, *Journal of Chemical Education*, 1968, **45**, 581.
90. R. G. Pearson, *Journal of Chemical Education*, 1968, **45**, 643.
91. C. Erlinger, D. Gazeau, T. Zemb, C. Madic, L. Lefrancois, M. Hebrant and C. Tondre, *Solvent Extraction and Ion Exchange*, 1998, **16**, 707-738.
92. M. R. Antonio, R. Chiarizia and F. Jaffrennou, *Separation Science and Technology*, 2010, **45**, 1689-1698.
93. Y. Chevalier and T. Zemb, *Reports on Progress in Physics*, 1990, **53**, 279-371.
94. P.-M. Gassin, R. Champory, G. Martin-Gassin, J.-F. Dufrêche and O. Diat, *Colloids and Surfaces A: Physicochemical and Engineering Aspects*, 2013, **436**, 1103-1110.
95. A. Paquet, O. Diat, L. Berthon and P. Guilbaud, *J. Mol. Liq.*, 2019, **277**, 22-35.
96. A. W. C. Penisson, J. Theisen, V. Kokoric, B. Mizaikoff, J.C.P. Gabriel, Anaheim, CA, USA, 2018.

View Article Online  
DOI: 10.1039/C9CP06569E



Table of content entry :

View Article Online  
DOI: 10.1039/C9CP06569E



A membrane based liquid-liquid extraction microfluidic device coupled with X-ray fluorescence, enables first quantification of free energies of transfer dependence for a complex mixture of rare earth elements and iron using synergic extractants.

